INTERPENETRATING PLASMA SHELLS: NEAR-EQUIPARTITION MAGNETIC FIELD GENERATION AND NON-THERMAL PARTICLE ACCELERATION

L. O. Silva $^{1,6},$ R. A. Fonseca 1, J. W. Tonge 2, J. M. Dawson 2 , W. B. $\rm Mori^{2,3},$ M. V. $\rm Medvedev~^{4,5}$

Draft version February 2, 2008

ABSTRACT

We present the first three-dimensional fully kinetic electromagnetic relativistic particle-in-cell simulations of the collision of two interpenetrating plasma shells. The highly accurate plasma-kinetic "particle-in-cell" (with the total of 10^8 particles) parallel code OSIRIS has been used. Our simulations show: (i) the generation of long-lived near-equipartition (electro)magnetic fields, (ii) non-thermal particle acceleration, and (iii) short-scale to long-scale magnetic field evolution, in the collision region. Our results provide new insights into the magnetic field generation and particle acceleration in relativistic and sub-relativistic colliding streams of particles, which are present in gamma-ray bursters, supernova remnants, relativistic jets, pulsar winds, etc..

Subject headings: magnetic fields – instabilities – acceleration of particles

1. INTRODUCTION

Various violent astrophysical phenomena, such as gamma-ray bursts (GRBs), supernova explosions, pulsar wind outflows, knots in relativistic jets, are known (or believed) to be rather strong sources of synchrotron radiation and cosmic rays, indicating the presence of nearequipartition magnetic fields and strong particle acceleration. These conditions are, in general, associated with shocks or regions with colliding streams of particles. How the magnetic fields are generated, how long do they live and how particles are accelerated are still open questions, which can only be definitely addressed via fully kinetic three-dimensional numerical simulations. Most astrophysical shocks are collisionless because dissipation is dominated by particle scattering in turbulent electromagnetic fields rather than particle-particle collisions (Sagdeev, 1966). Plasma instabilities driven by streaming particles are responsible for the excitation of these turbulent electromagnetic fields. The Weibel instability (Weibel, 1959) has received considerable interest as a possible robust mechanism for the production of sub-equipartition long-lived magnetic fields and energetic particles in GRBs (Medvedev & Loeb, 1999; Pruet et al., 2001) and pulsar winds (Kazimura et al., 1998). However, Gruzinov (2001a) put the simulation results of Kazimura et al. (1998) into question, claiming that the produced fields cannot survive far behind the shock. Previously, Arons and co-workers also pointed out the role of the Weibel instability in the downstream region of relativistic magnetosonic shocks (Langdon et al., 1988; Gallant et al., 1989).

In this Letter, we examine the dynamics of two colliding inter-penetrating unmagnetized plasma shells with zero net charge. This is the most simple model for the collision region of two plasma shells, as well as a clas-

sic scenario unstable to electromagnetic and/or electrostatic plasma instabilities. To probe the full nonlinear dynamics and the saturated state of this system it is necessary to employ kinetic numerical simulations. We use the fully electromagnetic relativistic particle-in-cell (PIC) code OSIRIS (Hemker, 2000; Fonseca et al., 2002) to perform the first three-dimensional kinetic simulations of the collision of two plasma shells, and to observe the three-dimensional features of the electromagnetic filamentation instability, or Weibel instability. We compare the collision of weakly-relativistic and ultra-relativistic plasma shells. We also point out the most distinct features of the three-dimensional simulations, not present in lower dimensional simulations. Finally, we discuss the key points raised by this work and the directions for future work.

2. SIMULATION MODEL

In this paper we illustrate the main features of the collision of two plasma shells, using the PIC code OSIRIS (Hemker, 2000; Fonseca et al., 2002). A general description of PIC codes is presented by Dawson (1980) and Birdsall & Langdon (1982). This scenario is pervasive in astrophysical scenarios, and it is of particular relevance in the early formation stages of collisionless shocks. Our simulations are directly relevant to internal shocks in gamma ray bursts, in connection with collisions of electron-positron fireball shells.

The simulations were performed on a $256 \times 256 \times 100$ grid (the axes are labeled as x1, x2, x3) with a total of 105 million particles for 2900 time steps, with periodic boundary conditions. A parameter scan was done in order to guarantee the grid resolution and the size of the simulation box do not affect the simulation results. Temporal and spatial scales in the simulations are normalized to the

¹GoLP/Centro de Fisica de Plasmas, Instituto Superior Técnico, 1049-001 Lisboa, Portugal

²Dept. of Physics and Astronomy, University of California, Los Angeles, CA 90095

³Dept. of Electrical Engineering, University of California, Los Angeles, CA 90095

⁴Canadian Institute for Theoretical Astrophysics, University of Toronto, Toronto, ON, M5S 3H8, Canada

⁵Present address: Department of Physics and Astronomy, University of Kansas, Lawrence, KS 66047

⁶email: luis.silva@ist.utl.pt

inverse electron plasma frequency $\omega_{pe}^{-1} = (4\pi e^2 n_e/m_e)^{1/2}$, and the collisionless skin depth $\lambda_e = c/\omega_{pe}$, where n_e is the electron-positron shell density; charges and masses are measured in the units of the electron charge e and the electron mass m_e . In these normalized units, the box size is $V=25.6\times25.6\times10.0\,(c/\omega_{pe})^3$, and the simulations ran for 150.0 ω_{pe}^{-1} . In all runs, energy is conserved down to 0.025 %. In our simulations, a charge-neutral plasma shell, consisting of electrons and positrons and moving with a bulk momentum $u_3 = \gamma_0 v_3/c$ along the x3 direction (vertical direction), penetrates into a similar plasma shell, moving in the opposite direction with the same momentum u_3 (here γ_0 is the initial Lorentz factor of the particles and v_3 is the bulk velocity of a shell along x3). Thus, at t=0 there are two groups of particles moving in opposite directions in the center of mass frame and occupying the entire simulation volume. The particles in both groups (shells) have a thermal spread with the rms momentum $u_{th} = \gamma_0 v_{th} \simeq 0.1$. The system has no net charge and no net current, and initially the electric and magnetic fields are set to zero. We performed both sub-relativistic ($u_3 = 0.6, \gamma_0 \approx 1.17,$ $v_{th} = 0.085c$) and ultra-relativistic ($u_3 = 10.0, \gamma_0 \approx 10.05,$ $v_{th} = 0.01c$) simulations. By using the mass ratio of 1 (electron-positron plasma), we can follow more clearly the crucial features of the instability process. Note that in the dimensionless units used, the results of the simulations are equally applicable to the collision of proton – antiproton shells as well. We have also performed collisions of electron-proton plasma shells and we have observed a two-stage instability process, with each stage evolving on the electron and proton collisionless time scales, following the pattern observed for the electron-positron shells (see Medvedev & Loeb (1999), and Tonge (2002)).

3. NUMERICAL RESULTS AND PHYSICAL PICTURE

The fundamental issue to be addressed here is the level of the electromagnetic field generated via plasma instabilities during the collision of two plasma shells, as well as the saturated state of the particles and fields. we show, the growth rate is so short that the saturated state is all that matters for astrophysical conditions. In Figure 1, we present the temporal evolution of the total energy in the produced magnetic and electric fields normalized to the initial total kinetic energy in the system (ϵ_p) , $\epsilon_B = \int B^2 dV/8\pi \epsilon_p$ and $\epsilon_E = \int E^2 dV/8\pi \epsilon_p$, for the sub-relativistic $(u_3 = 0.6)$ and ultra-relativistic $(u_3 = 10)$ scenarios. In our normalized units, the initial total kinetic energy of particles in the simulations is $\epsilon_p = 4 \times (\gamma_0 - 1) \times 10.0 \times (25.6)^2$. During the linear stage of the instability we observed the rapid generation of a strong magnetic field, which predominantly lies in the x1x2-plane, i.e., perpendicular to the direction of motion of the plasma shells. The magnetic field energy density reaches $\sim 5\%$ of ϵ_p for $u_3 = 0.6$ and $\sim 20\%$ for $u_3 = 10.0$. In all cases, the produced electric field is significantly weaker than the magnetic field. After the linear stage, the instability saturates and the energy in the magnetic field decays rapidly (on the collisionless time scale ω_{ne}^{-1}), until it reaches a quasi-steady level with no or very slow decay on a time scale much longer than ω_{pe}^{-1} . These features are present in both the weakly relativistic and ultra-relativistic conditions. Such long-lived magnetic

fields, associated with the Weibel instability, have also been observed in laboratory experiments (Lal et al., 1997). The linear growth rate agrees well with the theoretical estimates for the full electromagnetic instability (maximum growth rate, Γ , given by $(\Gamma/\omega_{pe})^2 \sim 2\beta_0^2/\gamma_0(1+\beta_{\rm th})^2$, for $\gamma_0 \gg 1$, and $\beta_{\rm th} \ll 1$) (Silva et al., 2002). Figure 1 also illustrates the main features of the Weibel instability, in particular, the linear growth rate scaling with $\gamma_0^{-1/2}$ and the scaling of the saturation level of the magnetic field with v_{th}^{-1} . The saturation level of the magnetic field, $B_{\rm sat}$, i.e., when B-field growth stalls, can be determined by combining the analytical results for Γ , and an estimate for the bounce frequency of the particles, ω_{bounce} , in the magnetic wells generated by the Weibel instability. Saturation occurs when $\Gamma \sim \omega_{\rm bounce}$, yielding $B_{\rm sat} \sim \sqrt{8\pi} m_p^{1/2} n_e^{1/2} \beta_0 c \gamma_0^{1/2}/(1+\beta_{\rm th})$, where $m_p(q_p)$ is the mass(absolute charge) of the particles in the cloud. Electron-proton clouds will drive higher levels of saturated B-field, by a factor of $(m_p/m_e)^{1/2}$ (Tonge, 2002), but on a longer time scale since $\Gamma \propto m_p^{-1/2}$. However, ϵ_B is independent of n_e , γ_0 and $m_p(q_p)$ (see also Medvedev & Loeb (1999) for a discussion). Thermal effects are known to play an important role in the evolution of the Weibel instability (Silva et al., 2002). Higher plasma temperatures will lead to a decrease of Γ and B_{sat} , and longer transverse wavelength filaments, within the orders of magnitude observed in our simulations (Silva et al. in preparation). The final steady-state level of the magnetic field is still quite high, up to 0.25\% of the initial total kinetic energy in the subrelativistic case and an order of magnitude higher in the ultra-relativistic conditions. This residual magnetic field is mostly perpendicular, i.e., the x1 and x2 components are dominant.

Physically, the inhomogeneities in the current will generate inhomogeneities in the magnetic field, which in turn will enhance the current inhomogeneities (thus closing the instability feedback loop), and generating a large number of current filaments with oppositely directed currents. The magnetic field associated with these currents has also a filamentary structure, as illustrated in Figure 2. In the early stages of the instability, one observes randomly distributed current and magnetic filaments. Figure 2a shows small-scale tilted iso-levels of the magnetic field energy density. When the instability enters the saturation phase $(t \approx 15 - 30 \ \omega_{pe}^{-1})$, current filaments begin to interact with each other, forcing like currents to approach each other and merge. During this phase, initially randomly oriented filaments cross each other to form a more organized, large-scale quasi-regular pattern. The strong decrease in the magnetic field energy is associated with a topological change in the structure of currents and magnetic fields, cf. Figure 2a, 2b, and 2c. After saturation $(t \gtrsim 30 \ \omega_{pe}^{-1})$, the filament coalescence continues, as indicated by the increase of the correlation scale, $\sim k^{-1}$, of the *B*-field in Figure 3. However, the spatial distribution of currents is now quite regular, so that filaments with opposite polarity no longer cross each other but simply interchange, staying always far away. The total magnetic field energy does not change any more. Note that the residual magnetic field is highly inhomogeneous, seen as a collection of magnetic field domains or "bubbles". The amplitude of the field in the bubbles is close to equipartition. Therefore, the overall decrease of the *B*-field energy is mostly associated with decreasing filling factor of the field. Note also that the magnetic domains separate current filaments of opposite polarity. The discussed temporal evolution can be easily followed in the magnetic field energy spectral density, Figure 3. The small-scale magnetic field is generated in the linear stage of the instability, attains its maximum value, and after saturation it evolves to larger length scales (i.e., smaller |k|) with the characteristic e-folding time $\sim \omega_B = eB/m_ec$ (Medvedev, in preparation); note that $\omega_B/\omega_{pe} = \sqrt{2\epsilon_B}$ and this is valid for relativistic particles as well.

The topological evolution of the magnetic field is accompanied by strong heating and non-thermal particle acceleration, as illustrated in Figure 4. Generation of nonthermal fast particles is more pronounced in the highest B-field scenarios. We have observed thermal (rms) momenta u_{th} as high as the initial bulk momentum u_3 . The magnetic field energy grows in the early stage by slowing down the plasma shells. Saturation is achieved by the combination of transverse energy spread and nearequipartition magnetic field generation. After saturation, the energy stored in the magnetic field is transferred back to the plasma particles, leading to strong heating and the generation of high energy tails in the distribution function, with energies up to $4(\gamma_0 - 1)$ for both sub-relativistic and ultra-relativistic plasma shells. The presence of such highenergy particles is fundamental to provide the mildly relativistic particles to be injected in other accelerating structures, such as collisionless shocks. Comparison of Figures 3 and 4 also shows that non-thermal particle acceleration and strong plasma heating are correlated with the topological evolution of the magnetic field when it evolves from small-scale structures to large-scale structures.

To elucidate the difference between the evolution in three dimensions vs. two dimensions, we performed several 2D runs using the same code: the runs in a plane parallel to the streaming velocity lead to an under-estimation of the magnetic field energy, while 2D runs in the plane perpendicular to the streaming direction of motion show suppression of the excitation of relativistic plasma waves along this direction and, hence, overestimate the magnetic field energy.

A critical question for the validity of the GRB synchrotron shock model (see, e.g., a review by Piran, 1999) is whether the magnetic field produced in the collision region survives for a sufficiently long time (e.g., comparable to the synchrotron cooling time), typically $\sim 10^5 \omega_{pe}^{-1}$ for prompt GRB emission and early afterglow and up to $\sim 10^{10} \omega_{pe}^{-1}$ for late (radio) afterglow, as measured in the collision frame. Our simulations show very weak or no field dissipation on time-scales $\sim 150~\omega_{pe}^{-1}$ in the collision region. In principle, on much longer time-scales, the *B*-field may be destroyed via reconnection. The back-of-the-envelope estimate of the reconnection time yields: $t_{rec} \sim (v_{rec}k)^{-1} \sim (0.1v_Ak)^{-1} \sim (0.1\epsilon_B^{1/2}k\lambda_e)^{-1} \sim 100(k\lambda_e)^{-1}$,

where $v_{rec} \sim 0.1 v_A$ is the reconnection velocity (Biskamp & Schwarz, 2001) and $v_A = B/(4\pi m_e n_e)^{1/2}$ is the electron Alfvén speed. Since k decreases with a shorter e-folding time $\sim 1/\sqrt{\epsilon_B} \sim 10$, reconnection slows down at large times and the field is able to survive for quite a while. In addition, a fundamental three-dimensional feature is the small tilting of current filaments. This is intrinsically three-dimensional and it is a manifestation of the coupling between the electromagnetic modes (\mathbf{k} in the x1x2-plane) and the electrostatic modes (\mathbf{k} parallel to the streaming velocity of the clouds), making magnetic field reconnection much more complicated (Silva et al. in preparation).

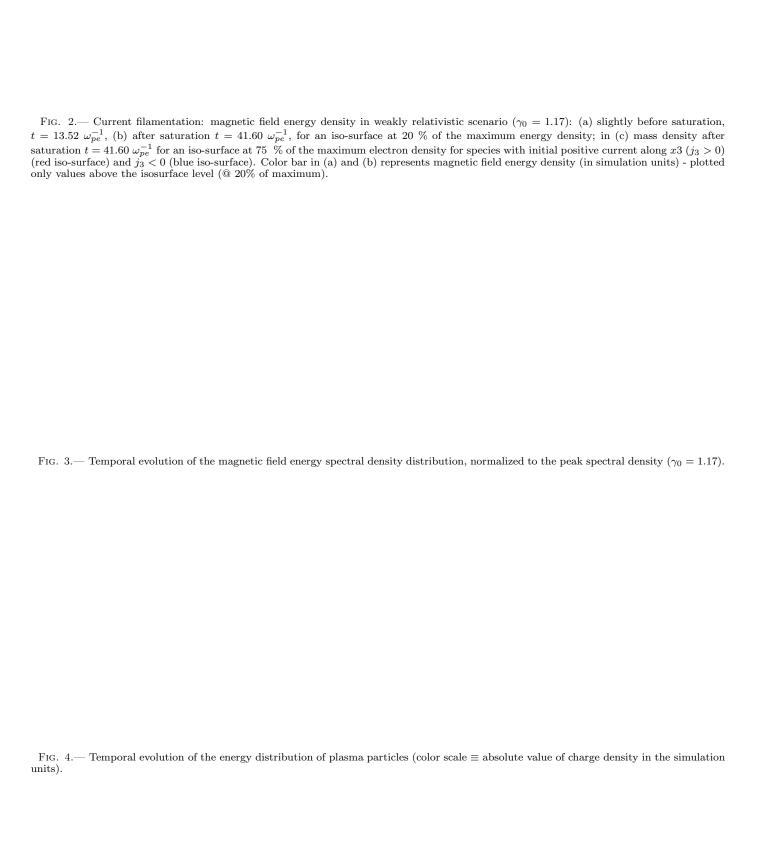
4. CONCLUSIONS

We presented the first self-consistent three-dimensional simulations of the fields present in collisions of plasma shells where the electromagnetic two-stream (or Weibel) instability develops. Our results demonstrate that this instability in three-dimensions is able to generate subequipartition quasi-static long-lived magnetic fields on the collisionless temporal and spatial scales in the collision region, giving credence to the predictions of Medvedev & Loeb (1999) and Pruet et al. (2001). After the linear stage of the instability, we first observe the decay of the magnetic field energy, as also observed by Gruzinov (2001b), followed by the evolution to a residual saturated magnetic field energy density. These fields maintain a strong saturated level on time-scales much longer than collisionless, at least for the duration of the simulations. The next step is to increase the simulation region spatial dimension in order to determine the spatial spread of the generated field. The obtained values of the equipartition parameter ($\epsilon_B \sim 3 \times 10^{-2} - 3 \times 10^{-3}$ for ultra- and subrelativistic shocks) agree well with the values of ϵ_B inferred from GRB afterglows (Panaitescu & Kumar, 2002). Furthermore, we show that strong transverse temperature increase and non-thermal particle acceleration occur when the instability saturates. The generated magnetic field evolves from small wavelengths to long wavelengths. Such a behavior may explain the observed evolution of the soft spectral index α in time-resolved GRB spectra (Ghirlanda et al., 2002; Medvedev (in preparation)) as a jitter-tosynchrotron spectral transition (Medvedev, 2000). Our results indicate that the fields necessary in the early formation stages of a shock front can be easily created via plasma instabilities of streaming plasmas. These simulations open the way to the full three-dimensional PIC modeling of relativistic collisionless shocks, which necessarily involve a different simulation geometry, and will be presented elsewhere.

This work was partially supported by FCT (Portugal) through grants PESO/PRO/40144/2000 and POCTI/33605/FIS/2000, and grants DOE DE-FGO3-98DP0021 and NSF PHY-0078508.

REFERENCES

Gruzinov, A. 2001, ApJ, 563, L15 Hemker, R. G. 2000, Ph.D. Thesis, UCLA Kazimura, Y., et al. 1998, ApJ, 498, L183 Lal, A. K., et al. 1997, Phys. Plasmas, 4, 1434 Langdon, A. B., et al. Phys. Rev. Lett., 61, 779 Medvedev, M. V. 2000, ApJ, 540, 704 Medvedev, M. V., & Loeb, A. 1999, ApJ, 526, 697 Panaitescu, A., & Kumar, P. 2002, ApJ, 571, 779 Piran, T. 1999, Phys. Rep., 314, 575 Pruet, J., Abazajian, K., & Fuller, G. 2001, Phys. Rev. D, 64, 063002 Sagdeev, R. Z. 1966, Rev. Plasma Phys., 4, 23 Silva, L. O., et al. 2002, Phys. Plasmas, 9, 2458 Tonge, J. W. 2002, Ph.D. Thesis, UCLA Weibel, E. S. 1959, Phys. Rev. Lett., 2, 83



This figure "figs.jpg" is available in "jpg" format from:

http://arXiv.org/ps/astro-ph/0307500v1